Journal of
Composites Science

MDPI

Article

Eco-Friendly Wall Cladding Panels from Recycled Fishing Gear and Clamshell Waste

Zakariae Belmokhtar [1,*], Patrice Cousin [1], Saïd Elkoun [2] and Mathieu Robert [1]

[1] Civil Engineering, Université de Sherbrooke, 2500, Boulevard de l'Université, Sherbrooke, QC J1K 2R1, Canada; patrice.cousin@usherbrooke.ca (P.C.); mathieu.robert2@usherbrooke.ca (M.R.)
[2] Mechanical Engineering, Université de Sherbrooke, 2500, Boulevard de l'Université, Sherbrooke, QC J1K 2R1, Canada; said.elkoun@usherbrooke.ca
* Correspondence: zakariae.belmokhtar@usherbrooke.ca; Tel.: +1-819-580-8073

Abstract: Eco-friendly wall cladding panels were developed from fishing industry waste by incorporating discarded ropes, wood fibers from lobster cages, and clamshell powder. Four panel formulations were investigated using MAPP and MAPE coupling agents: FRW-M (97% fishing rope), 30WF-M (67% rope with 30% wood fibers), 30CS-M (67% rope with 30% clamshell powder), and a hybrid 15CS15WF-M (67% rope with 15% each of wood fibers and clamshell powder). A DSC analysis revealed that clamshell powder addition reduced melting temperatures and crystallinity, while wood fiber incorporation led to slight increases in melting temperatures. The hybrid formulation exhibited enhanced crystallization temperatures despite lower overall crystallinity. A dynamic mechanical analysis showed an 85% improvement in storage modulus for the hybrid panel, with flexural testing demonstrating a 202% increase in modulus and 20% increase in strength. SEM-EDS analysis confirmed improved filler dispersion and interfacial adhesion in the hybrid formulation. Water absorption was lowest in FRW-M and highest in 30WF-M, while burning rate tests showed 30CS-M and 30WF-M as the best and worst performers, respectively. The hybrid formulation emerged as the optimal solution, combining enhanced mechanical properties with improved water resistance and fire retardancy, presenting a viable sustainable alternative for wall cladding applications.

Keywords: discarded ropes; clamshell powder; wood fibers; crystallinity

check for updates

Citation: Belmokhtar, Z.; Cousin, P.; Elkoun, S.; Robert, M. Eco-Friendly Wall Cladding Panels from Recycled Fishing Gear and Clamshell Waste. *J. Compos. Sci.* **2024**, *8*, 484. https://doi.org/10.3390/jcs8110484

Academic Editor: Salvatore Brischetto

Received: 28 September 2024
Revised: 11 November 2024
Accepted: 18 November 2024
Published: 20 November 2024

Copyright: © 2024 by the authors. Licensee MDPI, Basel, Switzerland. This article is an open access article distributed under the terms and conditions of the Creative Commons Attribution (CC BY) license (https://creativecommons.org/licenses/by/4.0/).

1. Introduction

Abandoned, lost, and discarded fishing gear (ALDFG) represents a significant source of oceanic plastic pollution, accounting for 46% of all floating plastic debris [1]. A meta-analysis by Richardson et al. [2] revealed that ALDFG comprises 6% net fragments, 9% pots, and 29% fishing lines, with annual losses of lobster traps ranging from 10 to 28% [3]. This lost gear causes severe ecological damage through passive mechanisms including ingestion, entanglement, and strangulation of marine species such as turtles, seabirds, dolphins, sharks, and seals [4]. In 2018 alone, over 300 sea turtles died from entanglement in hooks and nets [5].

Multiple factors contribute to fishing gear loss, including adverse weather conditions, gear entanglement, and substandard workmanship [6–8].

Island communities face challenges from ALDFG accumulation, with both environmental and economic implications due to their dependence on marine-oriented tourism. The Northern Hawaiian Islands exemplify this issue, where ALDFG accumulation along Pacific Ocean shorelines threatens numerous endangered species [9,10]. These communities also struggle with seashell waste management from fishing and seafood industries. Untreated shells, containing organic materials, generate foul odors and toxic gases (H_2S, NH_3, amines) [11] while attracting insects and pathogens like Escherichia coli and Salmonella [12,13]. Seashells primarily comprise calcium carbonate, which exists in three crystalline forms: calcite, aragonite, and vaterite. Calcite, the most stable and abundant

form, serves as a reference for aragonite and vaterite, which can transform into calcite under various conditions [14]. Scanning electron microscopy reveals distinct morphologies: rhombic for calcite and needle-like for aragonite [15]. The high aspect ratio of aragonite particles makes it particularly effective as a mechanical reinforcement in thermoplastic composites [16,17].

The Magdalen Islands (Îles de la Madeleine) in Quebec's Gulf of St. Lawrence exemplify these challenges. The islands generate 24.3 tons of fishing net and rope waste annually, alongside 100 tons of clamshell waste with disposal costs of $100 per ton as of 2019 [18]. The islands face another challenge related to housing shortage. Also, significant increase in housing demand due to tourism growth has reduced the availability of permanent housing. Building new homes is an urgent necessity to address this issue [19,20].

Previous research has explored ALDFG as a construction material resource, primarily as fiber reinforcement in various composites. Bertelsen and Ottosen [21] utilized fibers from fishing nets to reinforce gypsum-based materials, while Hussan et al. incorporated polyethylene and polypropylene fishing net fibers as reinforcement in cementitious composites [22]. As highlighted in a meta-analysis by Pablo Ojeda [23], most research has limited the application of fishing nets and ropes to be used as a filler in composite systems.

Previous research by the authors contributed to this field through the development of panels from discarded fishing ropes and evaluating their flexural and Izod impact properties in comparison to commercial panels [24]. However, no prior study, to the best of our knowledge, has focused on using fishing gear waste to produce composite cladding panels. This study aims to advance the field by developing eco-friendly wall panels that incorporate waste fishing ropes, clamshell powder from seafood processing, and wood fibers derived from crushed lobster cages. The implementation of these materials in isolated communities can reduce dependence on imported resources, lower waste management expenses, and contribute to easing local housing shortages.

2. Materials and Methods

2.1. Materials

CERMIM (Centre de recherche sur les milieux Insulaires et Maritimes) collected end-of-life fishing ropes from the Magdalen Islands' waste management center. The ropes, discarded after 2–3 years of service, underwent visual inspection to separate polyolefin ropes from nylon nets. On-site shredding was performed using a BM309 Pelletier Granulator (Granby, QC, Canada), with no preliminary washing step. A comprehensive characterization of these recovered fishing ropes was reported in our previous work [24].

Wood fibers were extracted from end-of-life lobster cages collected at various ports throughout the Madeleine Islands. The cages underwent mechanical processing using a Pelletier Model BM-309 granulator (Granby, QC, Canada), followed by overnight drying at 80 °C to eliminate moisture. Size classification through sieving retained fibers between 0.85 mm and 2 mm. Dimensional analysis using a Leica DMRX-POL photomicroscope, (Wetzlar, Hesse, Germany) conducted on 30 individual fibers, yielded an average aspect ratio (length-to-diameter ratio) of 8, with the fibers exhibiting an average density of 0.75 g/cm^3.

Clamshell powder was prepared from seafood processing waste collected from local island facilities. The shells underwent mechanical grinding, followed by a two-hour water boiling treatment to eliminate odors associated with organic matter decomposition. The treated powder was then oven-dried overnight at 120 °C. Characterization revealed a powder density of 3.15 g/cm^3 and a specific surface area of 37 cm^2/g.

Polypropylene-Graft-Maleic Anhydride (MAPP) and Polyethylene-Graft-Maleic Anhydride (MAPE) were obtained from Sigma Aldrich [25,26].

2.2. Panels Production Process

A HAAKE Polylab OS PTW 16 twin-screw extruder (16 mm screw diameter, 40:1 length-to-diameter ratio) (Waltham, MA, USA) was used for pellet production. The extrusion

process employed a temperature profile of 180 °C in the first zone and 190 °C in the remaining eight zones, with an operating speed of 70 rpm and 3 mm die diameter. Shredded fishing ropes underwent initial extrusion and pelletization, followed by mixing with formulation components (Table 1) and a second extrusion–pelletization cycle under identical conditions. The final pellets were uniformly distributed in a 200 × 200 × 3 mm^3 metallic mold and were compression molded using a 4533 AutoFour/3015-PL H Carver press (Wabash, IN, USA).

Table 1. Panel formulations by volume in percentage.

Panel	Fishing Rope	Wood Fiber	MAPP	MAPE	Clamshell Powder
FRW-M	97	0	1.5	1.5	0
30WF-M	67	30	1.5	1.5	0
30CS-M	67	0	1.5	1.5	30
15CS15WF-M	67	15	1.5	1.5	15

The compression molding consisted of two sequential cycles: hot-pressing at 190 °C for 10 min followed by cold-pressing at 30 °C for 10 min, both under 10 tons of pressure. The resulting four panel formulations are shown in Figure 1, with FRW-M serving as the control.

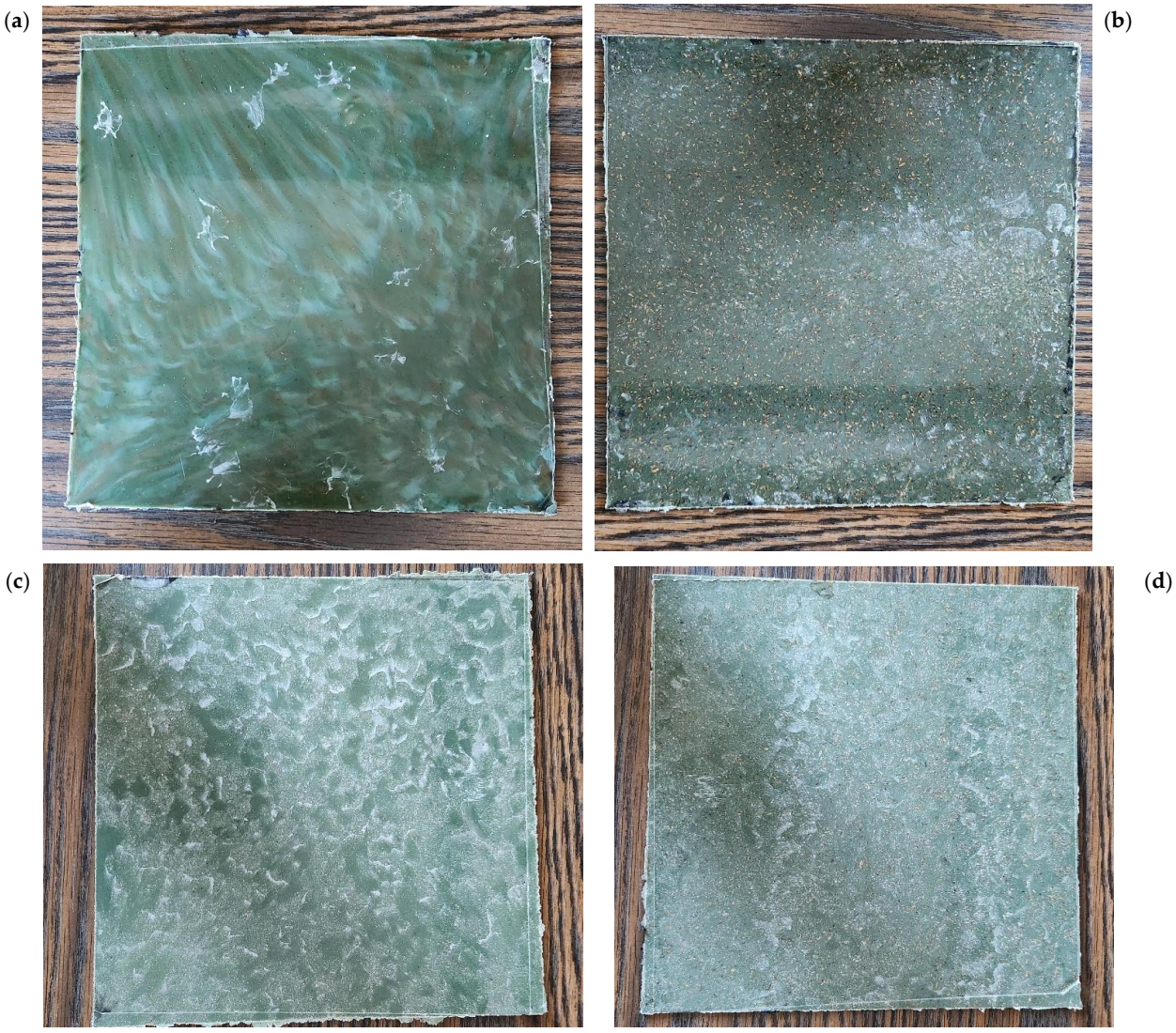

Figure 1. (**a**) FRW-M panel; (**b**) 30WF-M panel; (**c**) 30CS-M panel; (**d**) 15CS15WF-M panel.

2.3. Characterization of Clamshell Powder

2.3.1. Thermogravimetric Analysis (TGA)

Thermal decomposition behavior and the $CaCO_3$ content in clamshells were analyzed using TGA Dupont 2000 (Wilmington, DE, USA). Samples of 40 mg clamshell powder were heated from 30 °C to 900 °C at 20 °C/min under a nitrogen atmosphere.

The calcination process is an exothermic reaction where calcium carbonate transforms to calcium oxide (CaO) and carbon dioxide (CO_2) [27]. The percentage of calcium carbonate in the clamshell was estimated using Equation (1) [28]:

$$\%CaCO_3 = \frac{CaCO_{3\ MW}}{CaO_{\ MW}} \cdot CaO(\%) \quad (1)$$

where $CaCO_{3\ MW}$ and $CaO_{\ MW}$ are the molecular weight of calcium carbonate and calcium oxide, 100.08 g/mol and 56.07 g/mol, respectively [29,30]. CaO (%) denotes the percentage of calcium oxide in the clamshell powder determined from TGA analysis.

2.3.2. X-Ray Diffraction (XRD)

The crystalline structure of clamshell powder was analyzed using a Malvern Panalytical X'Pert Pro MPD diffractometer (Malvern, Worcestershire, UK). The XRD patterns were recorded from 2θ = 20° to 50° with a step size of 0.04°, using divergent and anti-scatter slits of 0.5° and 1°, respectively.

2.4. Characterization of the Panels

2.4.1. Differential Scanning Calorimetry (DSC)

The melting and crystallization behaviors of the polymer matrix were studied via differential scanning calorimetry using a DSC TA Instruments Q2000 (Newcastle, DE, USA). Samples of 15 mg underwent two thermal cycles from 0 °C to 200 °C at 10 °C/min, with a 1-min isothermal hold between cycles. Analysis was performed using data from the second thermal cycle.

The degree of crystallinity of matrix polymers was calculated using Equations (2) and (3):

$$\mathbf{XPP} = \frac{\Delta H_{\ m,pp}}{\Delta H_{\ m,\ 100pp} \cdot w_{pp}} \quad (2)$$

$$\mathbf{XHDPE} = \frac{\Delta H_{\ m,HDPE}}{\Delta H_{\ m,\ 100HDPE} \cdot w_{HDPE}} \quad (3)$$

where $\Delta H_{m,PP}$ and $\Delta H_{m,HDPE}$ are the melting enthalpies of PP or HDPE, and $\Delta H_{m,100PP}$ and $\Delta H_{m,100HDPE}$ are the melting enthalpy of 100% crystalline PP and HDPE, which are equal to 207 J/g and 293 J/g, respectively [31]. The fractions of PP and HDPE in the composite (w_{PP} and w_{HDPE}) were 0.75 and 0.25, respectively, based on previously determined rope composition [24]. The measurements were done on three samples per formulation, and the average thermal properties were reported.

2.4.2. Flexural Test

Flexural properties were measured according to ASTM D790-17 using a Zwick/Roell Z050 universal testing machine (Ulm, Baden-Württemberg, Germany). Five specimens (80 × 12.7 × 3 mm) from each panel were tested at a 1.2 mm/min crosshead speed with a 48 mm span [32].

2.4.3. Flammability Test

Flammability testing followed ASTM D635-22 standard [33] using specimens of 125 × 13 × 3 mm. The burning rate was calculated using Equation (4), where L repre-

sents the burned length between 25 and 100 mm marks, and t is the burning time in seconds. The test set-up is shown in Figure 2.

$$\textbf{Burning rate}(\textbf{mm/min}) = \frac{\textbf{60}\cdot \boldsymbol{L}(\boldsymbol{mm})}{\boldsymbol{t}(\boldsymbol{s})} \quad (4)$$

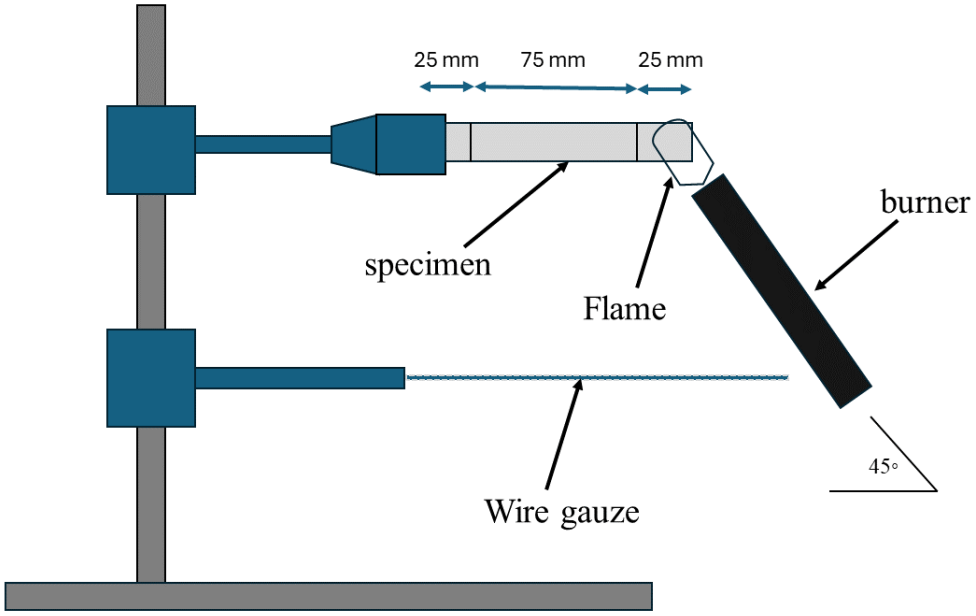

Figure 2. Flammability test set-up according to ASTM D635-22 [33].

2.4.4. Water Absorption Tests

Water absorption testing followed ASTM D570-22 [34] using specimens of 76.2 × 25.4 × 3 mm. Samples were immersed in distilled water at room temperature, with measurements taken daily for the first week and weekly thereafter until stabilization. Water uptake was calculated using Equation (5):

$$\textbf{Water uptake}(\%) = \frac{\boldsymbol{Wi} - \boldsymbol{Wo}}{\boldsymbol{Wo}} \cdot \textbf{100} \quad (5)$$

where W_i is the weight of the sample after immersion and W_0 is the weight of the sample before immersion. Three specimens were tested for each formulation, and the mean water absorption percentage was subsequently calculated.

2.4.5. Dynamic Mechanical Analysis (DMA)

A dynamic mechanical analysis was performed using DMA Q850 TA Instruments (Newcastle, DE, USA) in dual-cantilever mode. Tests were conducted at 1 Hz frequency from 25 °C to 200 °C at a 2 °C/min heating rate. Specimens (50 × 12.5 × 3 mm) were tested in triplicate for each panel formulation.

2.4.6. Scanning Electron Microscopy (SEM)

Fracture surface morphology was examined using JEOL NeoScope JCM-7000 SEM (Easton, MD, USA) at 15 kV, with magnifications of 30× for void analysis and 800× for interfacial adhesion assessment. EDS mapping of calcium distribution was performed on 30CS-M and 15CS15WF-M panels to evaluate clamshell powder dispersion within the matrix.

3. Results

3.1. Characterization of the Clamshell Powder

3.1.1. Thermogravimetric Analysis (TGA)

Thermogravimetric analysis of the clamshell powder (Figure 3) revealed distinct mass loss regions. No mass loss occurred between 0 and 200 °C, confirming the powder's initial dry state. Between 300 and 500 °C, a 1% mass loss corresponded to the decomposition of residual organic matter. A minor mass reduction between 500 and 600 °C indicated the aragonite-to-calcite phase transformation [35]. The most significant mass loss (45.03%) occurred between 600 and 800 °C, attributable to the calcination process converting calcium carbonate to calcium oxide and carbon dioxide [36].

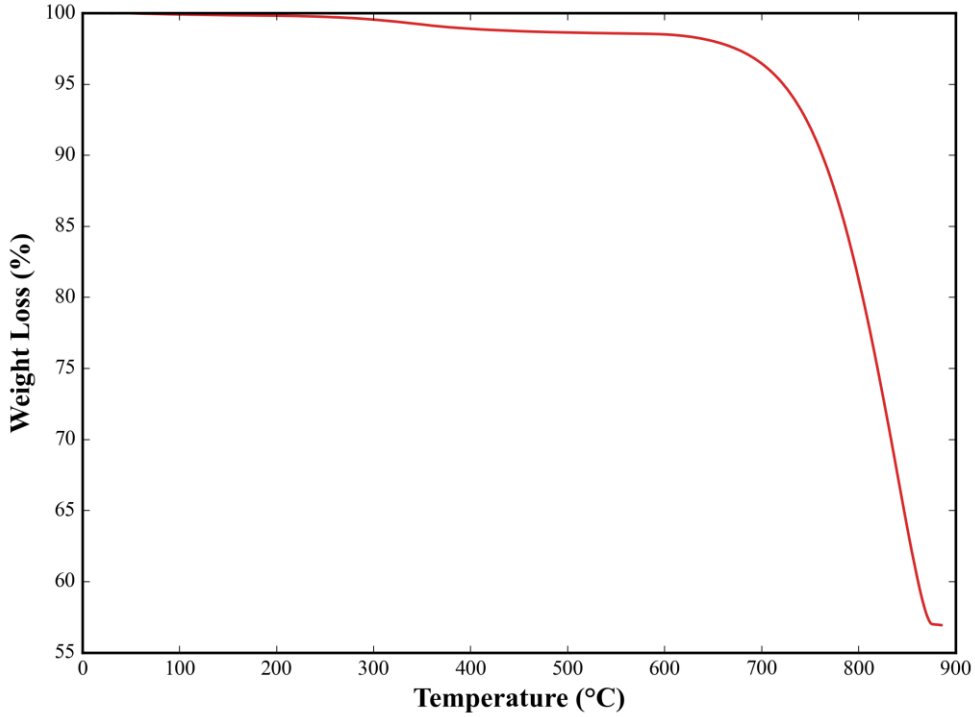

Figure 3. Thermogravimetric analysis of the clamshell powder.

Using Equation (1), the calculated $CaCO_3$ content of 98.1% aligns with previously reported values (92–99%) for seashell composition [37–39].

3.1.2. X-Ray Diffraction (XRD)

Figure 4 presents the XRD patterns of the clamshell. It can be observed that the dominant crystal structure is that of aragonite (JCPDS card No. 41-1475), with a minor peak corresponding to calcite (JCPDS card No. 47-1743), which may be due to the transformation of some aragonite crystals into calcite during the grinding process [17].

3.2. Characterization of the Panels

3.2.1. Differential Scanning Calorimetry (DSC)

Figure 5 and Table 2 present the DSC curves and thermal analysis data for the four formulations. The FRW-M formulation exhibits characteristic PP-HDPE blend behavior, featuring two distinct melting peaks and merged crystallization peaks due to the similar crystallization temperatures of HDPE and PP [40]. In the 30CS-M composite, the incorporation of clamshell powder reduces both the melting temperature and the crystallization degree of both polymers, indicating disrupted crystallization as particles occupy amorphous regions and inhibit crystal domain formation [41]. This results in smaller, less perfect spherulites, consistent with Zhang et al.'s [42] observations of calcium carbonate effects on

PP crystallization. The constant crystallization temperatures relative to FRW-M indicate that clamshell powder does not act as a nucleating agent [43].

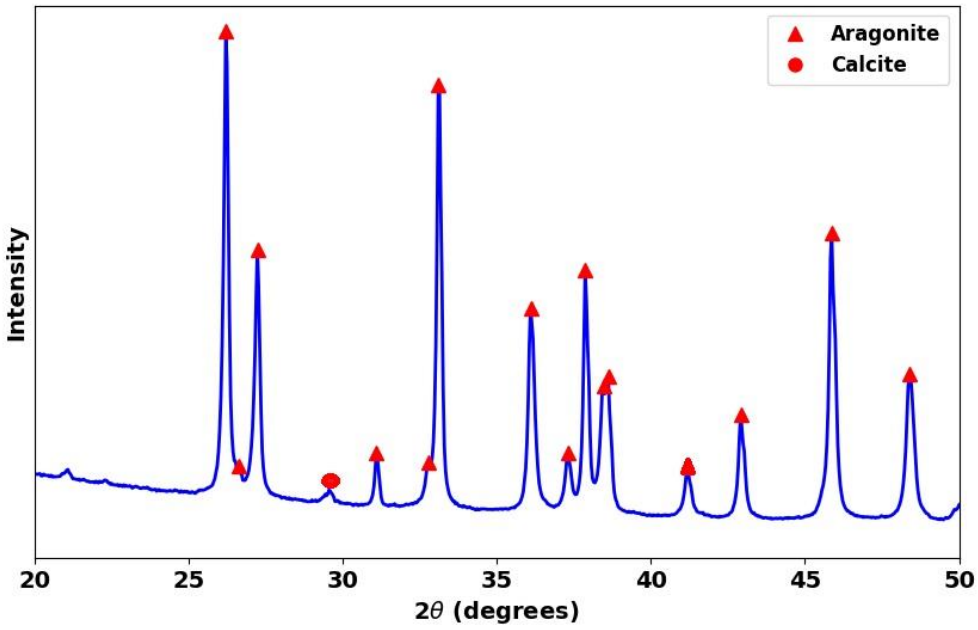

Figure 4. XRD of the clamshell powder.

Table 2. Melting temperature (Tm), crystallization temperature (Tc), melting enthalpy (ΔHm) and degree of crystallinity (X) for PP and HDPE of the four panels.

Samples	$\Delta H_{m,HDPE}$ (J/g)	$\Delta H_{m,PP}$ (J/g)	X_{HDPE} (%)	X_{PP} (%)	$T_{m,HDPE}$ (°C)	$T_{m,PP}$ (°C)	$T_{c,PP}$ (°C)	$T_{c,HDPE}$ (°C)
FRW-M	28	24	39.4	16	137.8	169.7	115	110.09
30CS-M	8	7	16.3	6.8	136	168.3	115.3	111.79
30WF-M	18	15	36.6	14.5	138.4	170.3	114.3	108.2
15CS15WF-M	14	15	28.5	14.5	138	170.4	115.6	112.3

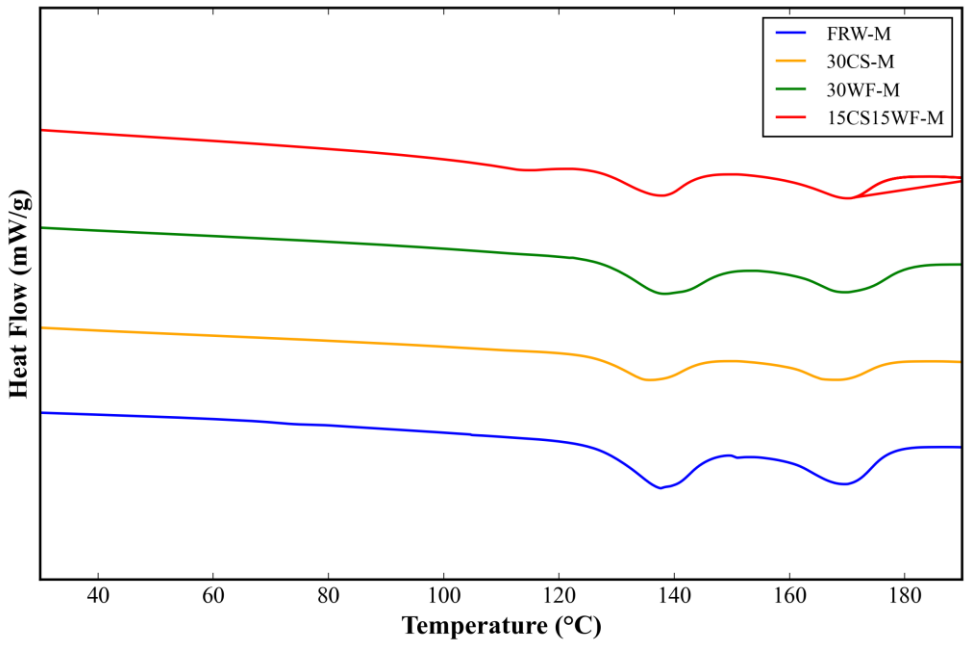

Figure 5. *Cont.*

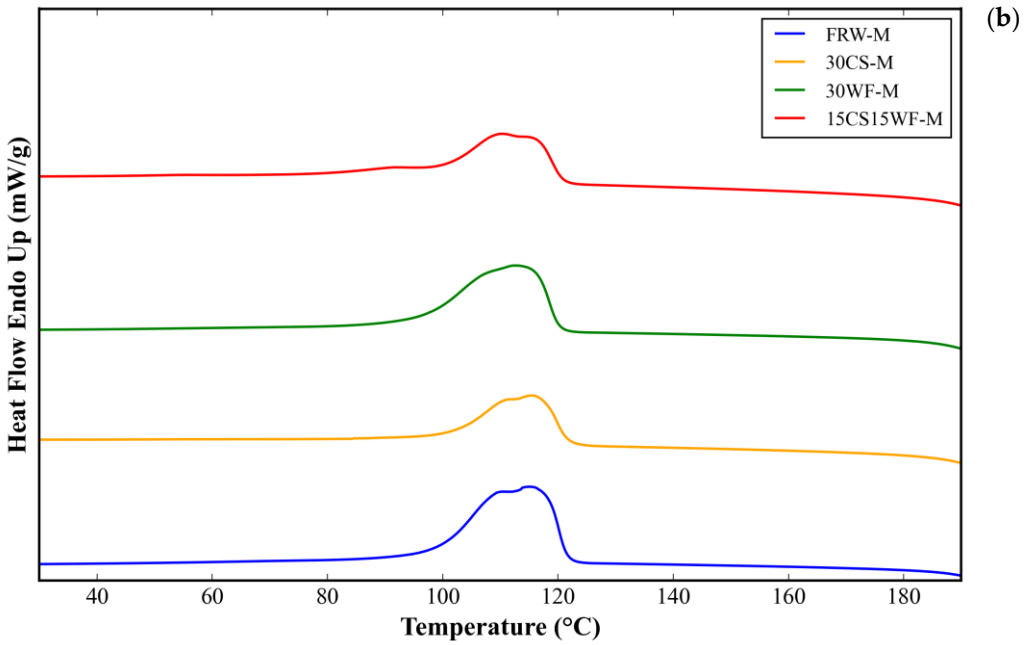

Figure 5. (**a**) Heating DSC curves of the panels; (**b**) cooling DSC curves of the panels.

The 30WF-M composite shows slightly reduced crystallinity degrees in both HDPE and PP, suggesting decreased spherulite size or nuclei density due to wood fibers restricting molecular chain movement, aligning with Wang et al.'s findings [44]. Despite this reduction, increased melting temperatures indicate more perfect spherulite formation, while decreased crystallization temperatures suggest that wood fibers impede matrix crystal rearrangement rather than provide nucleating effects [45].

The hybrid composite (15CS15WF-M) demonstrates intermediate behavior, with melting temperatures closer to FRW-M than 30CS-M, indicating a reduced impact on spherulite morphology due to better particle dispersion at lower clamshell content. The increased crystallization temperatures suggest enhanced nuclei density, potentially due to wood fiber nucleating effects and more effective coupling agent interactions at the lower wood fiber ratio. The decreased overall crystallinity likely results from competing mechanisms; while wood fibers appear to promote nuclei density, clamshell powder may simultaneously inhibit spherulite growth and nucleation. This proposed interaction could explain the observed moderate increase in nuclei density but substantially smaller spherulites, leading to reduced crystallinity degrees in both HDPE and PP.

3.2.2. Flexural Test

The flexural properties and corresponding curves for the four panels are presented in Figure 6 and Table 3. All composite formulations exhibited increased flexural modulus compared to FRW-M, with wood fibers and clamshell powder significantly enhancing panel stiffness. The hybrid composite (15CS15WF-M) showed the most substantial improvement with a 202% increase in modulus. This enhancement could be attributed to multiple factors; the reduced clamshell powder content (15% vs. 30%) minimized aggregate formation and improved dispersion, while the optimized wood fiber to coupling agent ratio enhanced fiber–matrix adhesion. The improved bonding mechanism involves maleic anhydride groups reacting with wood fiber hydroxyl groups to form ester bonds, while PP and PE components of MAPP and MAPE bond with the matrix. Conversely, 30WF-M likely suffered from insufficient coupling agent content, leading to inadequate fiber–matrix bonding, supported by DSC results indicating that wood fibers acted as nucleating agents only in the hybrid composite [46–49].

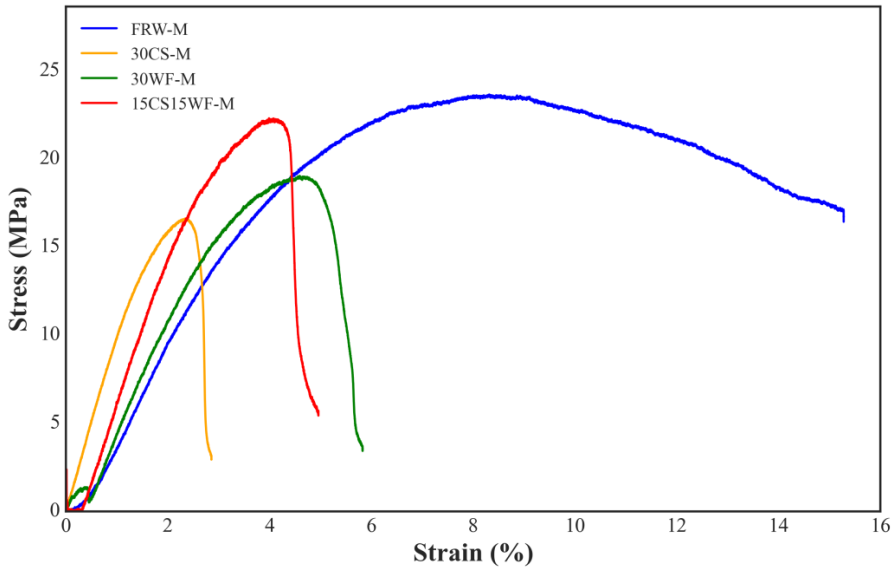

Figure 6. Flexural Stress–strain graph of the four panels.

Table 3. Flexural properties of the four panels.

Sample	Flexural Strength (Mpa)	Flexural Modulus (Gpa)	Elongation at Break (%)
FRW-M	23.33 ± 4.36	0.65 ± 0.20	15.15 ± 2.56
30CS-M	12.71 ± 1.56	1.03 ± 0.23	2.9 ± 0.35
30WF-M	16 ± 3.97	0.87 ± 0.19	5.98 ± 0.45
15CS15WF-M	27 ± 4.61	1.96 ± 0.58	4.86 ± 1.04

The 30% filler composites showed decreased flexural strength, with 30CS-M experiencing the largest reduction (43.11%). This decline may have resulted from an aggregate formation creating stress concentration points and poor interfacial adhesion limiting effective stress transfer. In contrast, the hybrid composite demonstrated a 20.86% increase in flexural strength. This enhancement likely results from an improved filler-matrix interface, reduced aggregate presence, and synergistic filler effects. The lower clamshell powder ratio may have facilitated matrix void filling, thereby reducing stress concentration points, while the wood fibers' higher aspect ratio potentially enhanced stress transfer.

Ductility measurements revealed significant reductions across all composite formulations compared to FRW-M. The 30CS-M showed the largest decrease in elongation at break (80.86%), followed by 15CS15WF-M (67.12%) and 30WF-M (60.51%). The substantial reduction in 30WF-M can be attributed to potential fiber agglomeration due to high loading, possibly leading to poor adhesion and restricted polymer chain mobility [50,51] For 30CS-M, the significant decrease is likely due to high-density clamshell powder causing particle agglomeration, which may restrict chain slippage [52].

The observed improvements in mechanical properties align with findings reported in previous studies on similar composite systems. Xu et al. demonstrated an 18% increase in flexural modulus when incorporating mussel shell powder into polypropylene [53], while Melo et al. reported enhanced flexural properties in HDPE composites containing mollusk shell powder [54]. In the context of wood fiber reinforcement, Yeshiwas et al. [55] established that wood fiber incorporation enhances the flexural strength of HDPE-PP composites for ceiling panel applications. Similarly, Srivabut et al. [56] achieved significant improvements in both flexural strength (25%) and modulus (12%) using a combination of recycled wood fiber and calcium carbonate powder in polypropylene composites. Notably, the hybrid composite developed in this study demonstrates superior performance compared to commercial alternatives, with its flexural modulus exceeding both MULFORD Plastics' HDPE cladding panel (1.37 GPa) [57] and SIMONA's HDPE panel (1.65 GPa) [58].

Figure 7 presents SEM micrographs at 30× magnification of the four panels. The FRW-M control sample exhibits a uniform surface without apparent voids, while the 30WF-M composite shows numerous voids resulting from poor interfacial adhesion, evidenced by fiber debonding and pull-out from the matrix. The 30CS-M sample similarly displays large surface voids, attributed to agglomerate formation that inhibited uniform polymer matrix distribution during molding. The hybrid composite (15CS15WF-M) demonstrates minimal void formation, reflecting enhanced interfacial adhesion and improved filler dispersion.

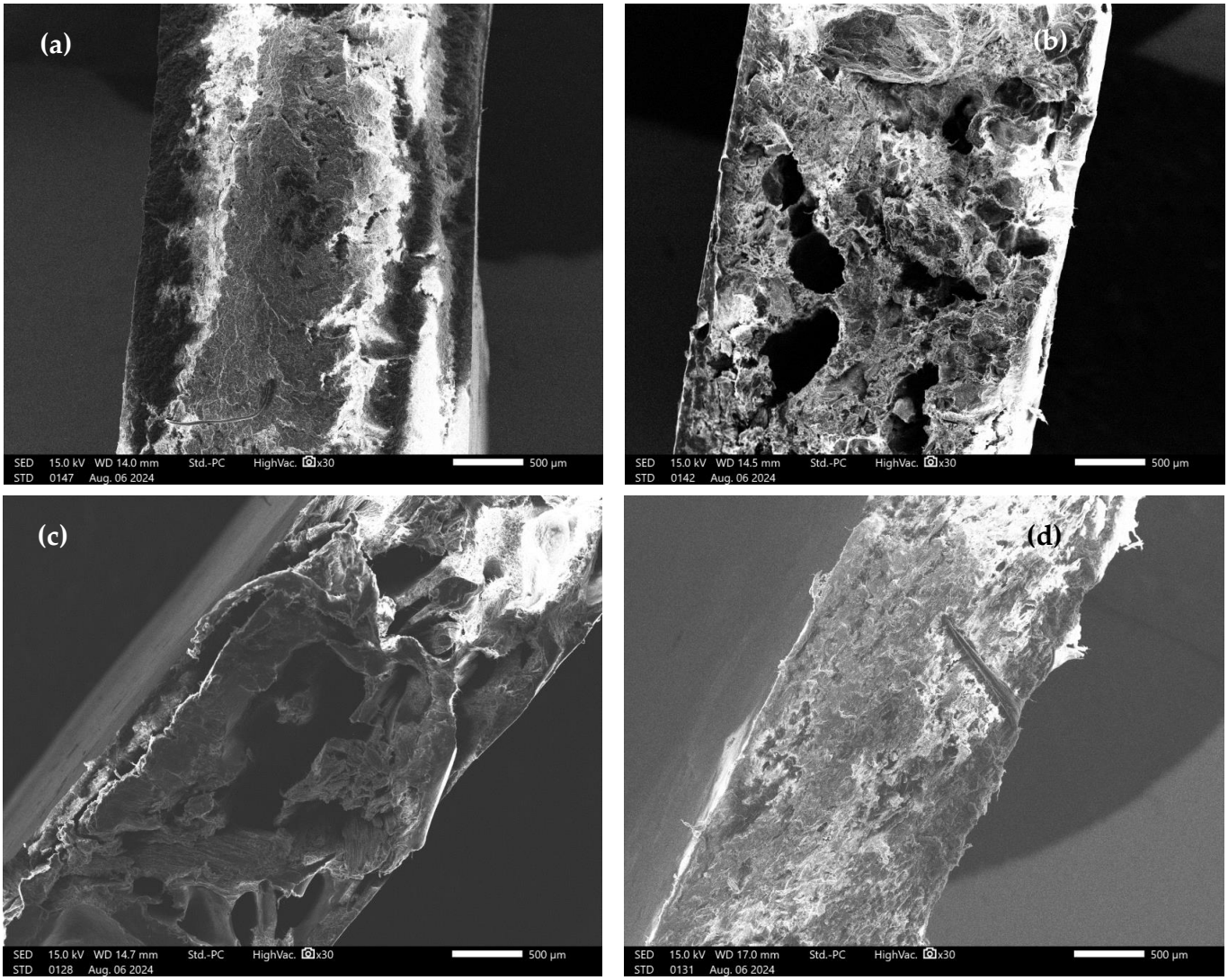

Figure 7. SEM micrographs at 30× magnification of (**a**) FRW-M sample; (**b**) 30CS-M sample; (**c**) 30WF-M sample; (**d**) 15CS15WF-M sample.

Higher magnification (800×) SEM analysis and EDS mapping (Figure 8) provide further insights into the compositional distribution and interfacial characteristics. EDS mapping reveals a higher concentration of clamshell particles (indicated by yellow dots) in the 30CS-M sample compared to 15CS15WF-M, consistent with its doubled clamshell powder content. Moreover, the 30CS-M sample shows inhomogeneous particle distribution, with notable concentration in the upper region, indicating aggregate formation. Comparative analysis of 30WF-M and 15CS15WF-M micrographs reveals significant differences in the fiber–matrix interaction. The 30WF-M sample exhibits fiber pull-out and surrounding voids, while the hybrid composite shows minimal void formation and no evidence of fiber pull-out, indicating superior interfacial adhesion attributed to more effective coupling agent activity.

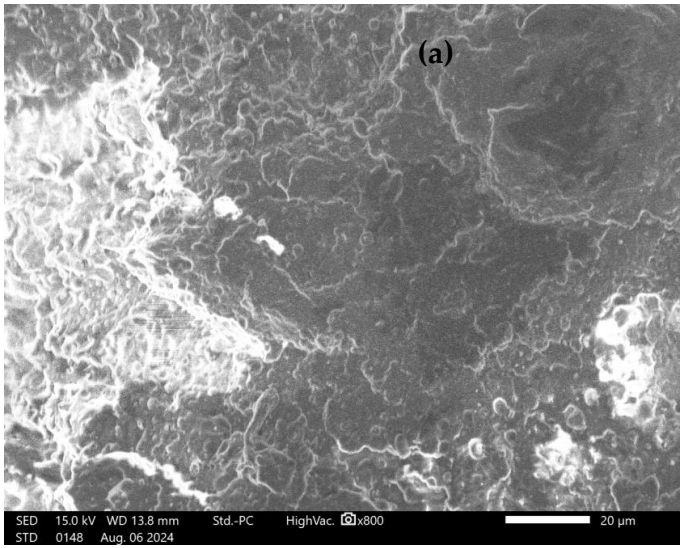

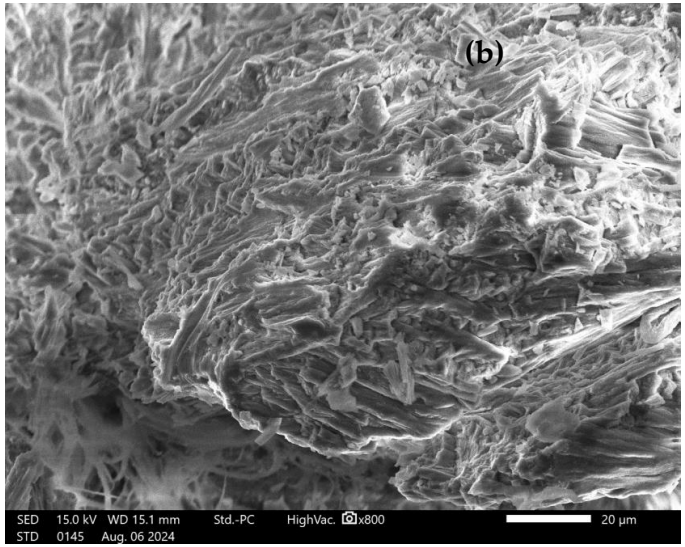

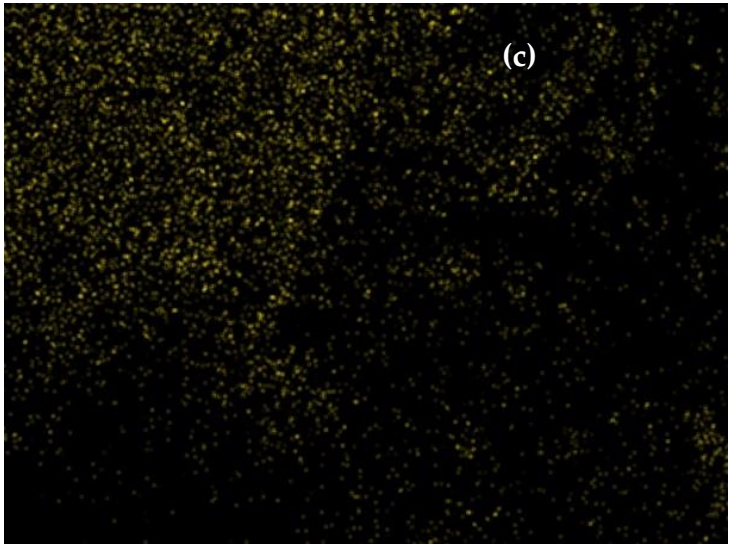

Figure 8. *Cont.*

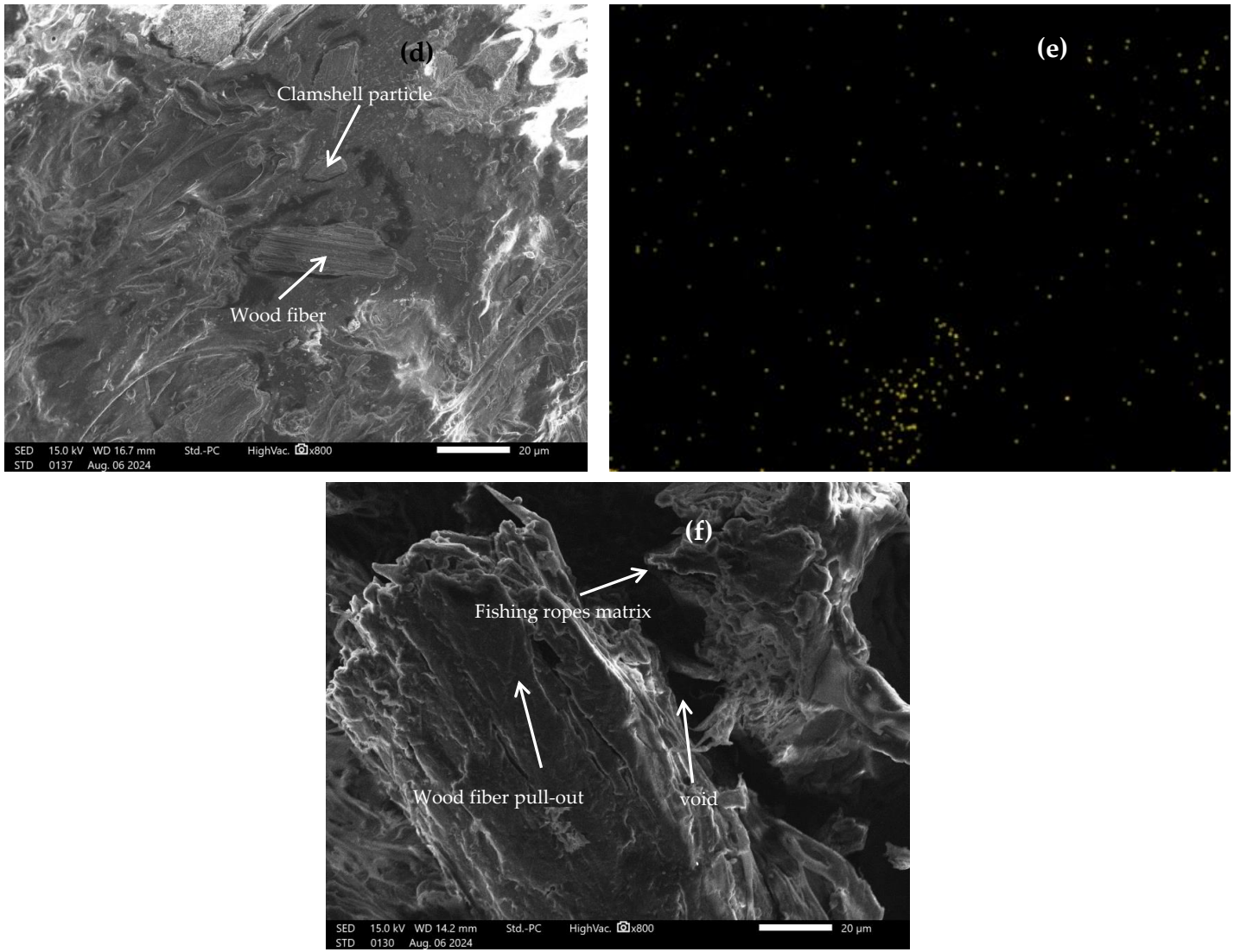

Figure 8. SEM micrographs at 800× magnification of (**a**) FRW-M sample; (**b**) 30CS-M sample; (**d**) 15CS15WF-M sample; (**f**) 30WF-M sample; Calcium EDS mapping of (**c**) 30CS-M; (**e**) 15CS15WF-M.

3.2.3. Dynamic Mechanical Analysis (DMA)

Figure 9 presents the dynamic mechanical analysis (DMA) results for the panel formulations. All panels exhibited a decrease in storage modulus with increasing temperature, beginning at approximately −20 °C, corresponding to the glass transition temperature of PP [59]. This modulus reduction stems from enhanced segmental motion in the amorphous regions of PP and HDPE, coupled with filler debonding from the polymer matrix [60]. The composite panels demonstrated superior stiffness compared to the control panel, with the hybrid composite (15CS15WF-M) showing the most significant improvement (85% increase in storage modulus at room temperature), followed by 30CS-M (48% increase) and 30FRW-M (18% increase). These improvements can be attributed to the reinforcing effect of the fillers enhancing stress transfer at the interface. The variations in performance among formulations correlate with differences in interfacial adhesion quality between the matrix and fillers, as confirmed by SEM analysis. These trends in storage modulus align with the observed flexural modulus results.

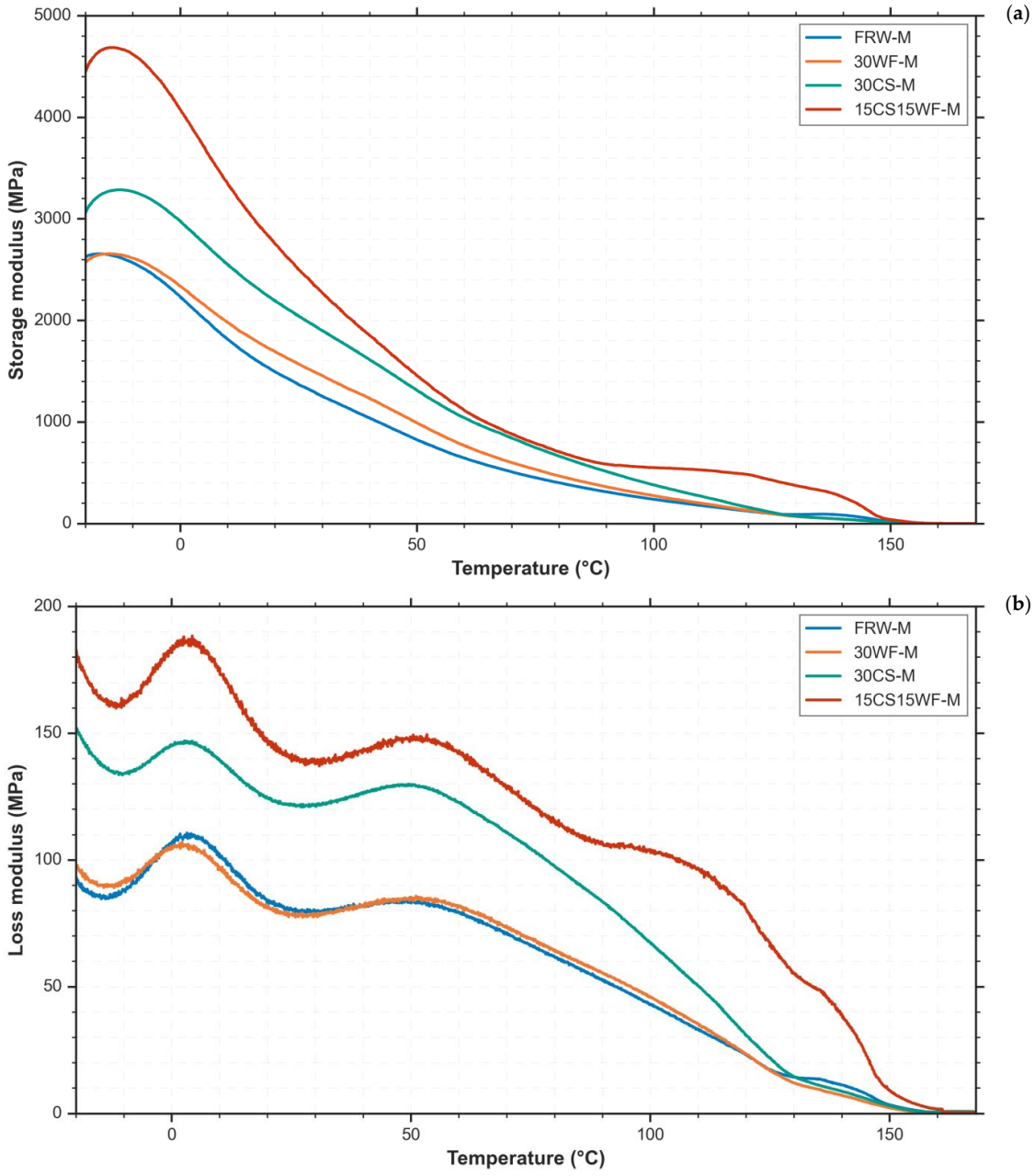

Figure 9. *Cont.*

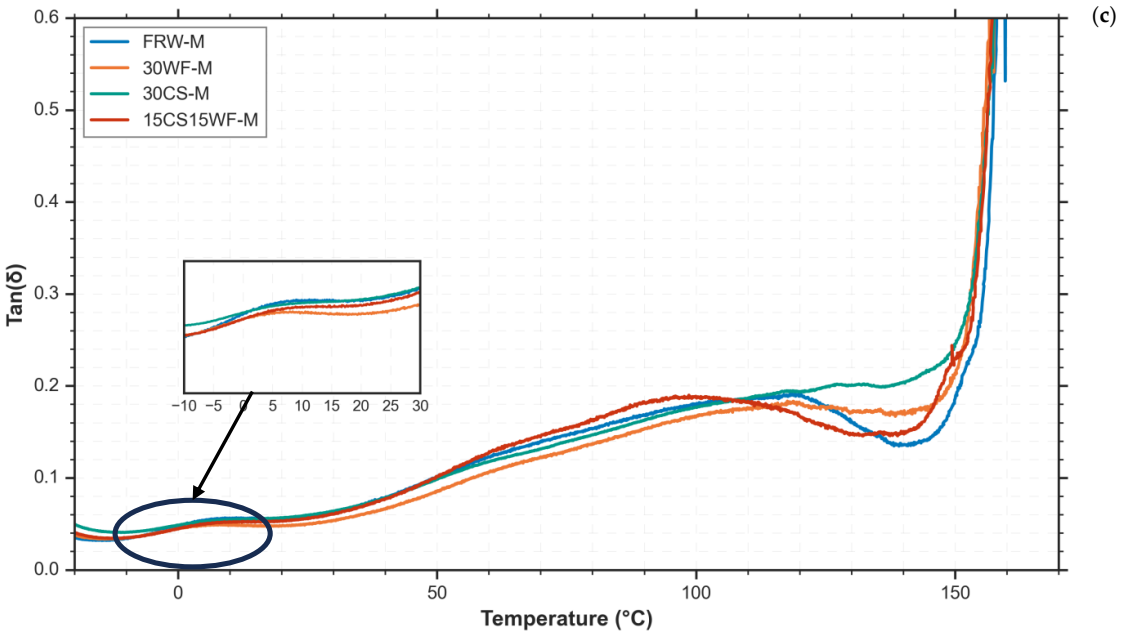

Figure 9. (**a**) Storage modulus of the four panels; (**b**) loss modulus of the four panels; (**c**) tan (δ) of the four panels.

The loss modulus curves exhibited patterns similar to the storage modulus across all formulations. A primary β-relaxation peak, corresponding to PP's glass transition, was observed at approximately 2 °C for most formulations [61]. However, the 30WF-M formulation showed a shift to −1 °C, attributed to wood fibers creating matrix gaps that increase free volume and facilitate chain movement near the fiber surfaces [62,63]. This observation is supported by SEM analysis, which revealed more surface gaps in 30WF-M compared to other formulations. The apparent temperature difference in PP's glass transition between storage and loss modulus measurements reflects the different measurement points used—onset of transition for storage modulus versus peak point for loss modulus [64]. The hybrid composite (15CS15WF-M) displayed two distinct peaks: one at 50 °C (α-relaxation of HDPE) and another at 110 °C (α-relaxation of PP) [65,66]. These peaks overlapped in the other formulations. The hybrid filler system demonstrated a more pronounced effect on PP's α-relaxation process, evidenced by increased peak intensity and a clearer separation between the PP and HDPE relaxation peaks. This enhancement likely results from strong filler–matrix adhesion restricting polymer chain mobility in crystallites near the fiber surfaces [67].

The tan δ results showed a 2 °C decrease in PP's glass transition temperature for the 30WF-M formulation, consistent with storage and loss modulus findings. Wood fiber-containing formulations (30WF-M and 15CS15WF-M) exhibited the lowest β-relaxation peak intensity, suggesting that wood fibers disrupted PP's crystalline structure and increased amorphous content, as confirmed by DSC analysis. The wood fibers appear to create physical constraints limiting amorphous segment motion, explaining both the reduced glass transition temperature and β-relaxation peak intensity [45,68]. The hybrid composite's tan δ exceeded other formulations above 30 °C but decreased below other composite panels near 90 °C, corresponding to PP's α-relaxation temperature peak. While this peak remained at 120 °C for other formulations, its shift in the hybrid composite likely results from reduced spherulite size caused by combined wood fiber and clamshell powder effects, as observed in the DSC analysis. This structural change created more interfacial area between PP's amorphous and crystalline regions, facilitating intracrystalline amorphous segment movement at lower temperatures. This aligns with Pluta and Kryszewski's [69] findings that smaller PP crystallites enhance mobility and relaxation within crystalline regions. The HDPE α-relaxation peak position remained constant at approximately 53 °C

across all formulations, likely due to HDPE's lower concentration in the matrix compared to PP.

3.2.4. Water Absorption Tests

Figure 10 illustrates the water absorption behavior of the four panel formulations over a 40-day period. The FRW-M composite exhibited the lowest water uptake (0.37% at day 40), attributed to the inherent hydrophobicity of its PP and HDPE components. Conversely, the 30WF-M formulation showed the highest water absorption at approximately 12% by day 40, primarily due to two factors: the hydrophilic nature of wood fibers and suboptimal fiber–matrix interfacial adhesion. The latter created voids at the fiber–matrix interface, facilitating water infiltration into the composite structure.

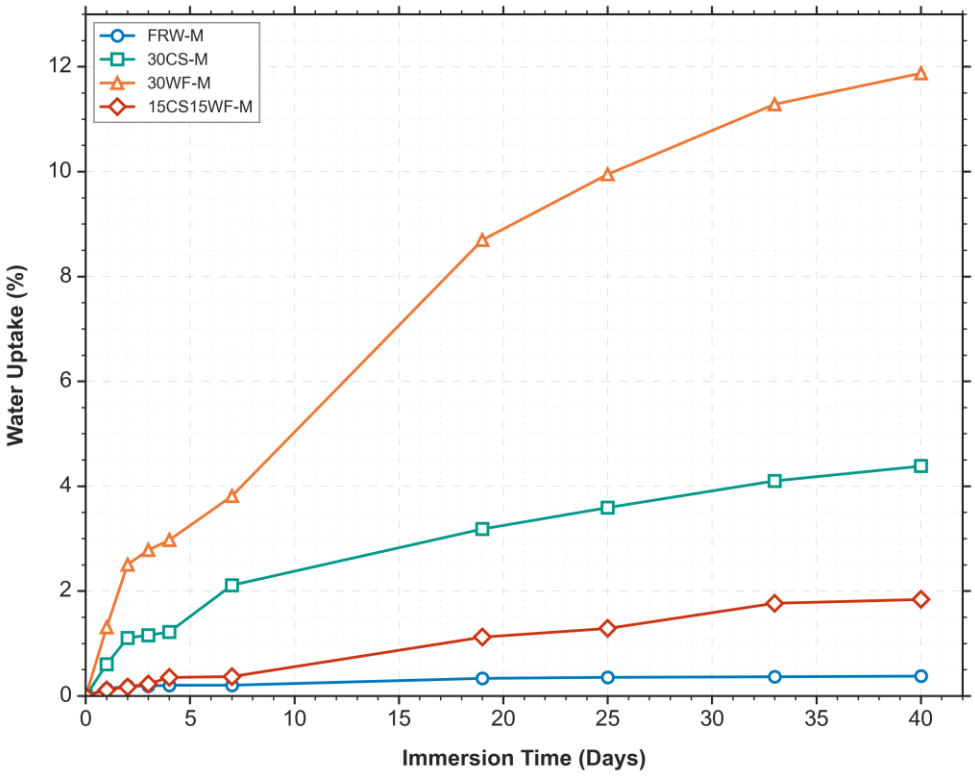

Figure 10. Water absorption of the panels.

The 30CS-M composite demonstrated intermediate water absorption behavior, reaching 4.5% at day 40. This moderate uptake can be attributed to two main factors: (1) the hydrophilic nature of calcium carbonate combined with the high specific surface area of the fine clamshell powder particles, which increased water molecule contact sites, and (2) poor interfacial adhesion between particles and the polymer matrix, resulting in void formation through aggregate clustering.

The hybrid composite (15CS15WF-M) showed superior water resistance compared to both the 30WF-M and 30CS-M formulations. This improved performance is attributed to two key factors: enhanced interfacial adhesion between the fillers and the matrix, resulting in reduced void formation and the lower volume fraction of each filler type, which minimized aggregate formation as confirmed by SEM analysis.

3.2.5. Flammability Test

Figure 11 presents the burning rate analysis of the four panel formulations. The 30CS-M formulation demonstrated superior fire resistance with the lowest burning rate (32.8 mm/min). This enhanced fire resistance can be attributed to two primary mechanisms: (1) the decomposition of $CaCO_3$ generates CO_2 during combustion, reducing oxygen

availability at the polymer surface and thereby inhibiting the combustion process [70], and (2) the high aspect ratio of aragonite particles in the shell powder facilitates the formation of a continuous charcoal network, effectively reducing flame propagation [71].

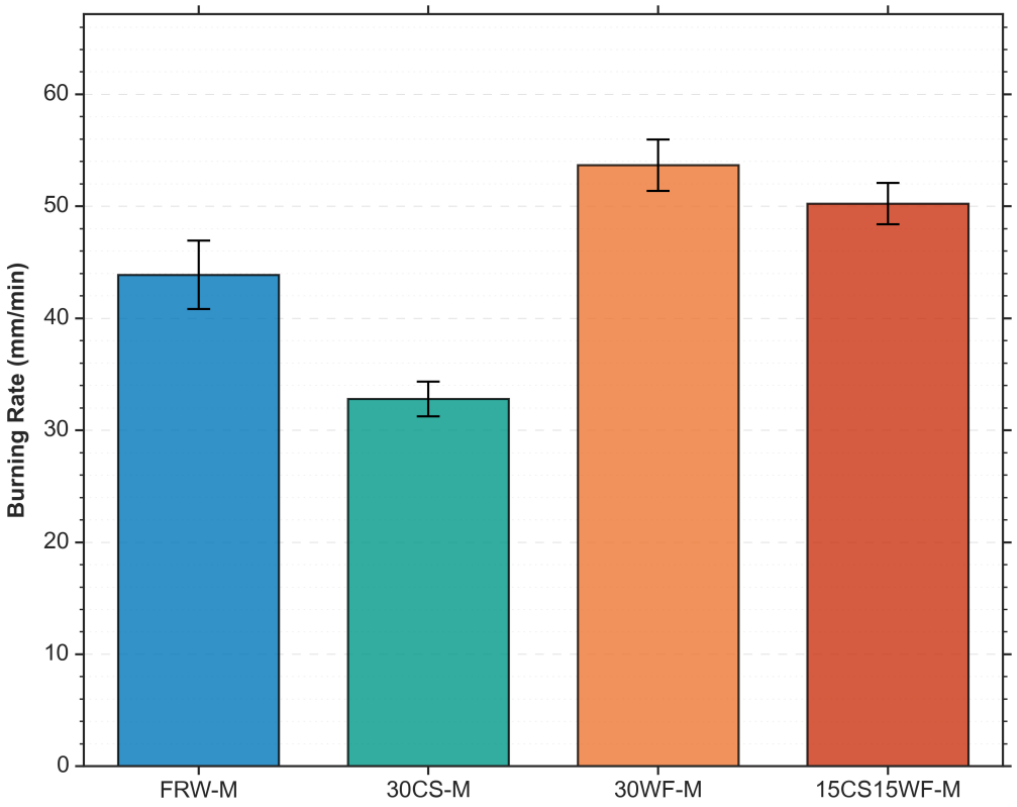

Figure 11. Burning rate of the panels.

In contrast, the 30WF-M formulation exhibited the highest burning rate (53.6 mm/min), a result consistent with the lower ignition temperature of dry wood fibers compared to both HDPE and PP matrix materials [72–74]. The hybrid composite (15WF15CS-M) showed intermediate fire resistance, with a burning rate lower than 30WF-M, reflecting both the fire-retardant contribution of the clamshell powder and the reduced wood fiber content in the formulation.

In polymer-based composites, dripping behavior plays a critical role in flame propagation, as molten droplets expose underlying materials to flames and accelerate fire spread [75]. Effective flame retardancy therefore requires both a low burning rate and minimal dripping tendency.

Figure 12 illustrates the distinct burning behaviors of the four formulations. The 30WF-M formulation demonstrated the poorest fire resistance, characterized by the largest flame size and highest dripping frequency, attributable to the high combustibility of wood fibers. Conversely, the 30CS-M formulation exhibited superior fire resistance, displaying both the smallest flame size and lowest dripping frequency. The presence of clamshell particles effectively delayed flame spread, evidenced by char formation (visible as a black area) in the combustion front zone, which inhibited continuous burning [76]. The hybrid composite (15CS15WF-M) exhibited intermediate fire resistance characteristics, with moderate flame size and dripping frequency, reflecting the balanced influence of its wood fiber and clamshell powder components.

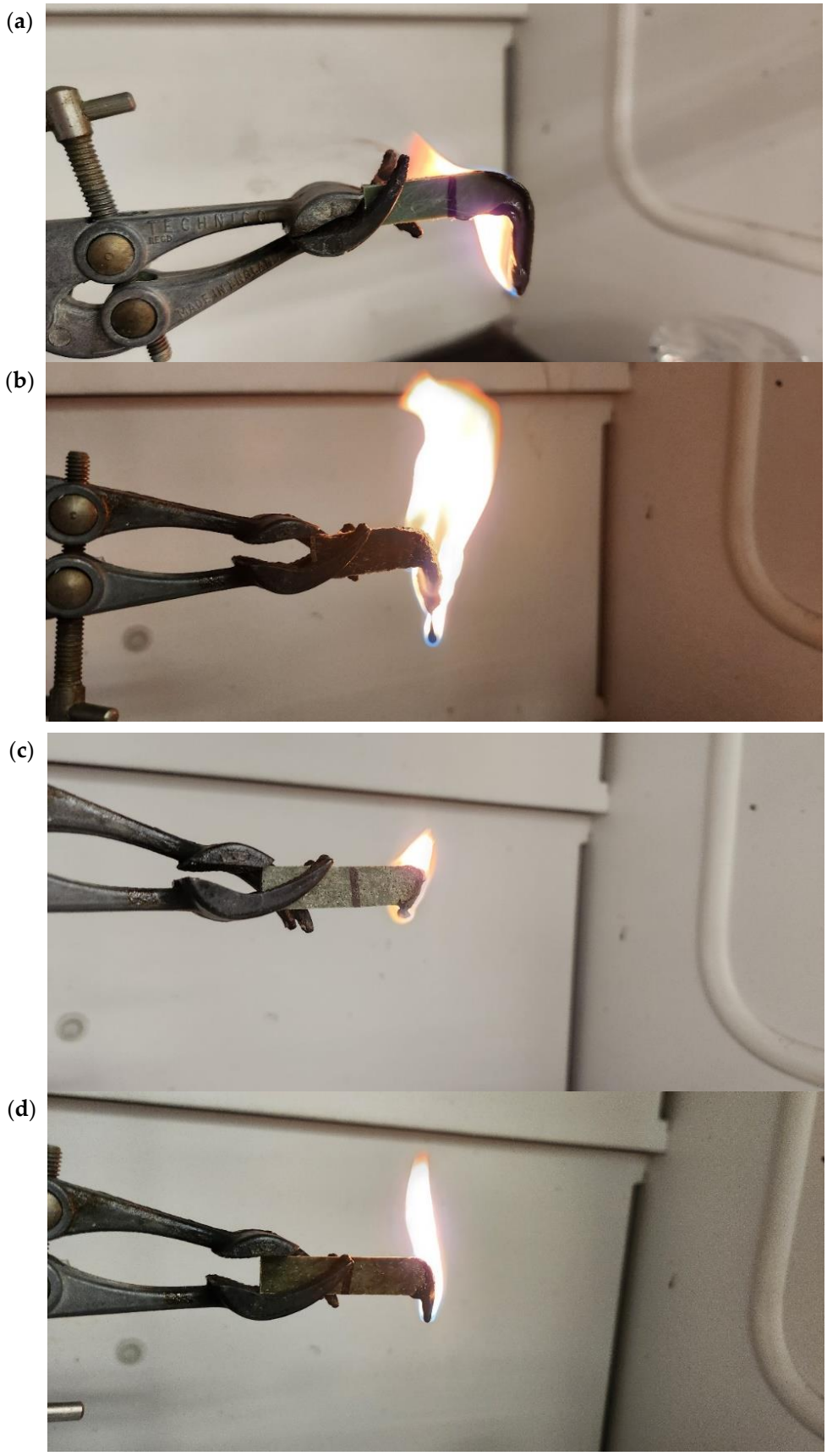

Figure 12. Burning behavior of (**a**) FRW-M sample; (**b**) 30WF-M sample; (**c**) 30CS-M sample; (**d**) 15CS15WF-M sample.

4. Conclusions

The present study has demonstrated the feasibility of valorizing fishing industry waste materials into sustainable wall cladding panels. The systematic investigation of four formulations revealed that the hybrid composite incorporating 15% clamshell powder and 15% wood fiber (15CS15WF-M) exhibited optimal performance characteristics. This formulation achieved significant improvements in mechanical properties, including a 202% increase in flexural modulus, 20% enhancement in flexural strength, and 85% higher storage modulus compared to the control. Microstructural analysis confirmed that these enhancements were attributable to improved filler dispersion and interfacial adhesion between components. Furthermore, the incorporation of clamshell powder contributed to enhanced fire resistance and reduced water absorption properties. These findings provide compelling evidence that fishing industry waste can be effectively repurposed into high-performance building materials, offering a sustainable solution to both waste management and construction material needs in coastal regions. Future research should focus on scaling up production and evaluating long-term durability under varied environmental conditions.

Author Contributions: Z.B. conceptualized the study, defined the methodology, collected and analyzed the data, and wrote the manuscript. M.R., P.C. and S.E. were involved in editing and reviewing the manuscript and provided funding for the research study. All authors have read and agreed to the published version of the manuscript.

Funding: Research was funded by MITACS, grant number IT39206.

Data Availability Statement: The original contributions of this study are included in the article. For further information, please contact the corresponding author.

Acknowledgments: The authors thank the Centre de Recherche sur les Milieux Insulaires et Maritimes (CERMIM) for providing the materials used in this study.

Conflicts of Interest: The authors declare no conflicts of interest.

References

1. Lebreton, L.; Slat, B.; Ferrari, F.; Sainte-Rose, B.; Aitken, J.; Marthouse, R.; Hajbane, S.; Cunsolo, S.; Schwarz, A.; Levivier, A.; et al. Evidence that the Great Pacific Garbage Patch is rapidly accumulating plastic. *Sci. Rep.* **2018**, *8*, 4666. [CrossRef]
2. Richardson, K.; Hardesty, B.D.; Vince, J.; Wilcox, C. Global estimates of fishing gear lost to the ocean each year. *Sci. Adv.* **2022**, *8*, eabq0135. [CrossRef] [PubMed]
3. Uhrin, A.V.; Matthews, T.R.; Lewis, C. Lobster Trap Debris in the Florida Keys National Marine Sanctuary: Distribution, Abundance, Density, and Patterns of Accumulation. *Mar. Coast. Fish.* **2014**, *6*, 20–32. [CrossRef]
4. Allsopp, M.; Walters, A.; Santillo, D.; Johnston, P. *Plastic Debris in the World's Oceans*; Greenpeace International: Amsterdam, The Netherlands, 2006. Available online: https://www.greenpeace.to/greenpeace/wp-content/uploads/2011/05/plastic_ocean_report.pdf. (accessed on 15 June 2024).
5. Markham, L. Endangered Olive Ridley Sea Turtles Found Dead in Mexico. Available online: https://www.nationalgeographic.com/animals/article/endangered-olive-ridley-sea-turtles-dead-mexico-news (accessed on 3 June 2024).
6. Azevedo-Santos, V.M.; Hughes, R.M.; Pelicice, F.M. Ghost nets: A poorly known threat to Brazilian freshwater biodiversity. *An. Acad. Bras. Cienc.* **2022**, *94*, e20201189. [CrossRef] [PubMed]
7. Macfadyen, G.; Huntington, T.; Cappell, R. Abandoned, lost or otherwise discarded fishing gear. In *UNEP Regional Seas Reports and Studies No. 185*; FAO Fisheries and Aquaculture Technical Paper No. 523; UNEP/FAO: Rome, Italy, 2009. Available online: https://www.researchgate.net/publication/242491383_Abandoned_Lost_or_Otherwise_Discarded_Fishing_Gear. (accessed on 3 June 2024).
8. Matthews, T. Assessing Opinions on Abandoned, Lost, or Discarded Fishing Gear in the Caribbean. 2009. Available online: https://www.researchgate.net/publication/228995317 (accessed on 20 June 2024).
9. Donohue, M.J.; Boland, R.C.; Sramek, C.M.; Antonelis, G.A. Derelict Fishing Gear in the Northwestern Hawaiian Islands: Diving Surveys and Debris Removal in 1999 Confirm Threat to Coral Reef Ecosystems. *Mar. Pollut. Bull.* **2001**, *42*, 1301–1312. [CrossRef] [PubMed]
10. Dameron, O.J.; Parke, M.; Albins, M.A.; Brainard, R. Marine debris accumulation in the Northwestern Hawaiian Islands: An examination of rates and processes. *Mar. Pollut. Bull.* **2007**, *54*, 423–433. [CrossRef]
11. Yoon, G.-L.; Kim, B.-T.; Kim, B.-O.; Han, S.-H. Chemical–mechanical characteristics of crushed oyster-shell. *Waste Manag.* **2003**, *23*, 825–834. [CrossRef]

12. Bee, S.-L.; Hamid, Z. Hydroxyapatite derived from food industry bio-wastes: Syntheses, properties and its potential multifunctional applications. *Ceram. Int.* **2020**, *46*, 17149–17175. [CrossRef]
13. Das, K.C.; Minkara, M.Y.; Melear, N.D.; Tollner, E.W. Effect of Poultry Litter Amendment on Hatchery Waste Composting. *J. Appl. Poult. Res.* **2002**, *11*, 282–290. [CrossRef]
14. Ni, M.; Ratner, B.D. Differentiating calcium carbonate polymorphs by surface analysis techniques—An XPS and TOF-SIMS study. *Surf. Interface Anal.* **2008**, *40*, 1356–1361. [CrossRef]
15. Feng, Q.; Pu, G.; Pei, Y.; Cui, F.; Li, H.; Kim, T. Polymorph and morphology of calcium carbonate crystals induced by proteins extracted from mollusk shell. *J. Cryst. Growth* **2000**, *216*, 459–465. [CrossRef]
16. Jing, Y.; Nai, X.; Dang, L.; Zhu, D.; Wang, Y.; Dong, Y.; Li, W. Reinforcing polypropylene with calcium carbonate of different morphologies and polymorphs. *Sci. Eng. Compos. Mater.* **2018**, *25*, 745–751. [CrossRef]
17. Li, H.-Y.; Tan, Y.-Q.; Zhang, L.; Zhang, Y.-X.; Song, Y.-H.; Ye, Y.; Xia, M.-S. Bio-filler from waste shellfish shell: Preparation, characterization, and its effect on the mechanical properties on polypropylene composites. *J. Hazard. Mater.* **2012**, *217–218*, 256–262. [CrossRef] [PubMed]
18. Richard, O.; Thibodeau, M.; Massé, M.-O.; Beaudoin-Gagnon, M.-H.; Cummings, I.; Rabenasolo, H. Valorisation Agricole des Coquilles de Palourdes: Mise en Place de la Filière de Valorisation (Phase 3). Centre de Recherche sur les Milieux Insulaires et Maritimes (CERMIM), Îles-de-la-Madeleine (Québec). 46 p. + Annexes. 2019. Available online: https://www.cermim.ca/wp-content/uploads/2023/08/191220_Rapport-FINAL_Coquilles_Redacted.pdf (accessed on 12 November 2024).
19. Journal de Montréal. Forcée de Déménager 11 Fois en 6 Ans: La Pénurie de Logements Est Criante Aux Îles-de-la-Madeleine. Available online: https://www.journaldemontreal.com/2023/03/24/forcee-de-demenager-11-fois-en-6-ans-la-penurie-de-logements-est-criante-aux-iles-de-la-madeleine (accessed on 15 June 2024).
20. Radio-Canada. Pénurie de Logement Aux Îles-de-la-Madeleine: Un Eté 2022 Critique Pour le Service D'aide au Logement. Available online: https://ici.radio-canada.ca/nouvelle/1901679/penurie-logement-iles-de-la-madeleine-ete-2022-service-aide-logement (accessed on 15 June 2024).
21. Bertelsen, I.M.G.; Ottosen, L.M. Recycling of Waste Polyethylene Fishing Nets as Fibre Reinforcement in Gypsum-based Materials. *Fibers Polym.* **2022**, *23*, 164–174. [CrossRef]
22. Hussan, A.; Sebaibi, N.; El Haddaji, B.; Zelloufi, M. Comparative Effects of Polyethylene and Polypropylene-Based Waste Fishing Gear Fibers on Mechanical Parameters and Porosity of Cementitious Materials. In Proceedings of the RILEM Spring Convention and Conference 2024, Milan, Italy, 7–12 April 2024; pp. 132–140. [CrossRef]
23. Ojeda, J.P. A meta-analysis on the use of plastic waste as fibers and aggregates in concrete composites. *Constr. Build. Mater.* **2021**, *295*, 123420. [CrossRef]
24. Belmokhtar, Z.; Sanchez-Diaz, S.; Cousin, P.; Elkoun, S.; Robert, M. Polyolefin-Based Cladding Panels from Discarded Fishing Ropes: A Sustainable Solution for Managing Fishing Gear Waste in Isolated Islands. *Waste* **2024**, *2*, 337–353. [CrossRef]
25. Sigma Aldrich. Polyethylene-Graft-Maleic Anhydride. Available online: https://www.sigmaaldrich.com/CA/en/product/aldrich/456632 (accessed on 29 May 2024).
26. Sigma Aldrich. Polypropylene-Graft-Maleic Anhydride. Available online: https://www.sigmaaldrich.com/CA/en/product/aldrich/427845 (accessed on 29 May 2024).
27. Hyatt, E.P.; Cutler, I.B.; Wadsworth, M.E. Calcium Carbonate Decomposition in Carbon Dioxide Atmosphere. *J. Am. Ceram. Soc.* **1958**, *41*, 70–74. [CrossRef]
28. Owuamanam, S.; Cree, D. Progress of Bio-Calcium Carbonate Waste Eggshell and Seashell Fillers in Polymer Composites: A Review. *J. Compos. Sci.* **2020**, *4*, 70. [CrossRef]
29. Patnaik, P. Handbook of inorganic chemicals. *Choice Rev. Online* **2003**, *40*, 40–6428. [CrossRef]
30. PubChem. Calcium Carbonate. Available online: https://pubchem.ncbi.nlm.nih.gov/compound/Calcium-carbonate (accessed on 29 May 2024).
31. Blaine, R.L. *Polymer Heats of Fusion*; Thermal Applications Note TN048; TA Instruments: New Castle, DE, USA, 1990. Available online: https://www.tainstruments.com/pdf/literature/TN048.pdf (accessed on 29 May 2024).
32. *ASTM D790-17*; Standard Test Methods for Flexural Properties of Unreinforced and Reinforced Plastics and Electrical Insulating Materials. ASTM International: West Conshohocken, PA, USA, 2017.
33. *ASTM D635-22*; Standard Test Method for Rate of Burning and/or Extent and Time of Burning of Plastics in a Horizontal Position. ASTM International: West Conshohocken, PA, USA, 2022.
34. *ASTM D570-22*; Standard Test Method for Water Absorption of Plastics. ASTM International: West Conshohocken, PA, USA, 2022.
35. Qu, T.; Yao, X.; Owens, G.; Gao, L.; Zhang, H. A sustainable natural clam shell derived photocatalyst for the effective adsorption and photodegradation of organic dyes. *Sci. Rep.* **2022**, *12*, 2988. [CrossRef]
36. Shariffuddin, J.H.; Yean, W.C.; Ghazali, S.S. Investigating the catalytic properties of calcium compounds derived from marine based shell waste for wastewater treatment. *Mater. Today Proc.* **2018**, *5*, 21718–21727. [CrossRef]
37. Barros, M.; Bello, P.; Bao, M.; Torrado, J. From waste to commodity: Transforming shells into high purity calcium carbonate. *J. Clean. Prod.* **2009**, *17*, 400–407. [CrossRef]
38. Yao, Z.; Chen, T.; Li, H.; Xia, M.; Ye, Y.; Zheng, H. Mechanical and thermal properties of polypropylene (PP) composites filled with modified shell waste. *J. Hazard. Mater.* **2013**, *262*, 212–217. [CrossRef]

39. Moustafa, H.; Youssef, A.M.; Duquesne, S.; Darwish, N.A. Characterization of bio-filler derived from seashell wastes and its effect on the mechanical, thermal, and flame retardant properties of ABS composites. *Polym. Compos.* **2017**, *38*, 2788–2797. [CrossRef]
40. Aumnate, C.; Rudolph, N.; Sarmadi, M. Recycling of Polypropylene/Polyethylene Blends: Effect of Chain Structure on the Crystallization Behaviors. *Polymers* **2019**, *11*, 1456. [CrossRef]
41. Sahebian, S.; Zebarjad, S.; Khaki, J.V.; Sajjadi, S. The effect of nano-sized calcium carbonate on thermodynamic parameters of HDPE. *J. Mech. Work. Technol.* **2009**, *209*, 1310–1317. [CrossRef]
42. Zhang, Q.-X.; Yu, Z.-Z.; Xie, X.-L.; Mai, Y.-W. Crystallization and impact energy of polypropylene/$CaCO_3$ nanocomposites with nonionic modifier. *Polymer* **2004**, *45*, 5985–5994. [CrossRef]
43. Huang, L.; Wang, H.; Wang, W.; Wang, Q.; Song, Y. Non-isothermal crystallization kinetics of wood-flour/polypropylene composites in the presence of β-nucleating agent. *J. For. Res.* **2016**, *27*, 949–958. [CrossRef]
44. Wang, W.; Liu, L.; Ding, N.; Zhang, R.; Yu, J. Mechanical and thermal behavior analysis of wood–polypropylene composites. *Text. Res. J.* **2021**, *91*, 347–357. [CrossRef]
45. Cui, Y.; Tao, J.; Noruziaan, B.; Cheung, M.; Lee, S. DSC Analysis and Mechanical Properties of Wood—Plastic Composites. *J. Reinf. Plast. Compos.* **2010**, *29*, 278–289. [CrossRef]
46. Demir, H.; Atikler, U.; Balköse, D.; Tıhmınlıoğlu, F. The effect of fiber surface treatments on the tensile and water sorption properties of polypropylene–luffa fiber composites. *Compos. Part A Appl. Sci. Manuf.* **2006**, *37*, 447–456. [CrossRef]
47. Wu, C. Improving Polylactide/Starch Biocomposites by Grafting Polylactide with Acrylic Acid–Characterization and Biodegradability Assessment. *Macromol. Biosci.* **2005**, *5*, 352–361. [CrossRef]
48. Tserki, V.; Matzinos, P.; Kokkou, S.; Panayiotou, C. Novel biodegradable composites based on treated lignocellulosic waste flour as filler. Part I. Surface chemical modification and characterization of waste flour. *Compos. Part A Appl. Sci. Manuf.* **2005**, *36*, 965–974. [CrossRef]
49. Ndiaye, D.; Tidjani, A. Effects of coupling agents on thermal behavior and mechanical properties of wood flour/polypropylene composites. *J. Compos. Mater.* **2012**, *46*, 3067–3075. [CrossRef]
50. Ndiaye, D.; Gueye, M.; Diop, B. Characterization, Physical and Mechanical Properties of Polypropylene/Wood-Flour Composites. *Arab. J. Sci. Eng.* **2012**, *38*, 59–68. [CrossRef]
51. Chua, P.S. Dynamic mechanical analysis studies of the interphase. *Polym. Compos.* **1987**, *8*, 308–313. [CrossRef]
52. Bakly, N.S.; Al-Mutairi, N.H.; Layla, A.A.; Almaamori, M.H. Investigate the Effect of Temperature Change on the Properties of the PP/$CaCO_3$ Composites: A Comparative Study. *Al-Mustaqbal J. Sustain. Eng. Sci.* **2024**, *1*, 1. [CrossRef]
53. Xu, J.; Mucalo, M.R.; Pickering, K.L. Bioinspired surface modification of mussel shells and their application as a biogenic filler in polypropylene composites. *Compos. Part C Open Access* **2024**, *15*, 100520. [CrossRef]
54. Melo, P.M.A.; Macêdo, O.B.; Barbosa, G.P.; Ueki, M.M.; Silva, L.B. High-density polyethylene/mollusk shell-waste composites: Effects of particle size and coupling agent on morphology, mechanical and thermal properties. *J. Mater. Res. Technol.* **2019**, *8*, 1915–1925. [CrossRef]
55. Yeshiwas, T.A.; Yigezu, B.S.; Desalegn, Y.M. Investigation on the Mechanical Properties of Wood-Plastic Composites for theApplication of Ceiling Panels. *Mater. Res. Express* **2024**, *11*, 085304. [CrossRef]
56. Srivabut, C.; Ratanawilai, T.; Hiziroglu, S. Effect of nanoclay, talcum, and calcium carbonate as filler on properties of composites manufactured from recycled polypropylene and rubberwood fiber. *Constr. Build. Mater.* **2018**, *162*, 450–458. [CrossRef]
57. Mulford Plastics. HDPE Leaflet. Available online: https://www.mulfordplastics.com.au/media/1257/hdpe-leaflet.pdf (accessed on 4 June 2024).
58. SIMONA AMERICA INDUSTRIES. SIMONA® HDPE POLYTONE® SHEET. Available online: https://www.simona-america.com/fileadmin/user_upload/USA/Applications/Outdoor/Playground/16_SIMONA-HDPE-Polytone.pdf (accessed on 4 June 2024).
59. Lu, Q.-C.; Dou, Q. Investigation on microstructures, melting and crystallization behaviors, mechanical and processing properties of β-isotactic polypropylene/$CaCO_3$ toughening masterbatch composites. *J. Polym. Res.* **2017**, *24*, 206. [CrossRef]
60. Bassyouni, M. Dynamic mechanical properties and characterization of chemically treated sisal fiber-reinforced polypropylene biocomposites. *J. Reinf. Plast. Compos.* **2018**, *37*, 1402–1417. [CrossRef]
61. Biswal, M.; Mohanty, S.; Nayak, S.K. Mechanical, thermal and dynamic-mechanical behavior of banana fiber reinforced polypropylene nanocomposites. *Polym. Compos.* **2011**, *32*, 1190–1201. [CrossRef]
62. White, R.P.; Lipson, J.E.G. Polymer Free Volume and Its Connection to the Glass Transition. *Macromolecules* **2016**, *49*, 3987–4007. [CrossRef]
63. Turnbull, D.; Cohen, M.H. Free-Volume Model of the Amorphous Phase: Glass Transition. *J. Chem. Phys.* **1961**, *34*, 120–125. [CrossRef]
64. Tajvidi, M.; Falk, R.H.; Hermanson, J.C. Effect of natural fibers on thermal and mechanical properties of natural fiber polypropylene composites studied by dynamic mechanical analysis. *J. Appl. Polym. Sci.* **2006**, *101*, 4341–4349. [CrossRef]
65. Zhang, D.; Guo, J.; Zhang, K. Effects of compatilizers on mechanical and dynamic mechanical properties of polypropylene–long glass fiber composites. *J. Thermoplast. Compos. Mater.* **2015**, *28*, 643–655. [CrossRef]
66. Huang, R.; Xu, X.; Lee, S.; Zhang, Y.; Kim, B.-J.; Wu, Q. High Density Polyethylene Composites Reinforced with Hybrid Inorganic Fillers: Morphology, Mechanical and Thermal Expansion Performance. *Materials* **2013**, *6*, 4122–4138. [CrossRef]
67. Hristov, V.; Vasileva, S. Dynamic Mechanical and Thermal Properties of Modified Poly(propylene) Wood Fiber Composites. *Macromol. Mater. Eng.* **2003**, *288*, 798–806. [CrossRef]

68. John, M.J.; Anandjiwala, R.D. Chemical modification of flax reinforced polypropylene composites. *Compos. Part A Appl. Sci. Manuf.* **2009**, *40*, 442–448. [CrossRef]
69. Pluta, M.; Kryszewski, M. Studies of α relaxation process in spherulitic and nonspherulitic samples of isotactic polypropylene with different molecular ordering. *Acta Polym.* **1987**, *38*, 42–52. [CrossRef]
70. Hassen, A.A.; Dizbay-Onat, M.; Bansal, D.; Bayush, T.; Vaidya, U. Utilization of Chicken Eggshell Waste as a Bio-Filler for Thermoplastic Polymers: Thermal and Mechanical Characterization of Polypropylene Filled with Naturally Derived $CaCo_3$. *Polym. Polym. Compos.* **2015**, *23*, 653–662. [CrossRef]
71. Deodhar, S.; Shanmuganathan, K.; Fan, Q.; Wilkie, C.A.; Costache, M.C.; Dembsey, N.A.; Patra, P.K. Calcium carbonate and ammonium polyphosphate-based flame retardant composition for polypropylene. *J. Appl. Polym. Sci.* **2011**, *120*, 1866–1873. [CrossRef]
72. PRODUCT SAFETY INFORMATION SHEET. 2022. Available online: www.borealisgroup.com (accessed on 6 June 2024).
73. Shi, L.; Chew, M.Y.L. Experimental study of woods under external heat flux by autoignition. *J. Therm. Anal. Calorim.* **2012**, *111*, 1399–1407. [CrossRef]
74. QUADRANT ENGINEERING PLASTIC PRODUCTS. Material Safety Data Sheet. Available online: https://www.alro.com/dataPDF/Plastics/PlasticsMSDS/MSDS_HDPE.pdf (accessed on 6 June 2024).
75. Karlsson, L.; Lundgren, A.; Jungqvist, J.; Hjertberg, T. Influence of melt behaviour on the flame retardant properties of ethylene copolymers modified with calcium carbonate and silicone elastomer. *Polym. Degrad. Stab.* **2009**, *94*, 527–532. [CrossRef]
76. Rasib, S.Z.M.; Mariatti, M.; Atay, H.Y. Effect of waste fillers addition on properties of high-density polyethylene composites: Mechanical properties, burning rate, and water absorption. *Polym. Bull.* **2021**, *78*, 6777–6795. [CrossRef]

Disclaimer/Publisher's Note: The statements, opinions and data contained in all publications are solely those of the individual author(s) and contributor(s) and not of MDPI and/or the editor(s). MDPI and/or the editor(s) disclaim responsibility for any injury to people or property resulting from any ideas, methods, instructions or products referred to in the content.